Supplement of Earth Syst. Sci. Data, 17, 1851–1871, 2025
https://doi.org/10.5194/essd-17-1851-2025-supplement

Supplement of

Glacier-level and gridded mass change in river sources in the eastern Tibetan Plateau region (ETPR) from the 1970s to 2000

Yu Zhu et al.

Correspondence to: Shiyin Liu (shiyin.liu@ynu.edu.cn)

Supplementary Texts

S1. Comparative analysis with Topo DEM with ICESat-2 in off-glacier region

ICESat-2 ATL06 data (October 2018 - February 2019) were used to further evaluate the Topo DEM in stable off-glacier regions (Fig. S1). ATL06 boasts high accuracy, with horizontal and vertical uncertainties of less than 10 m and 3 mm, respectively (Smith et al., 2020; Brunt et al., 2019). While the mean elevation differences between ATL06-SRTM and SRTM-Topo were close to zero below 5,700 m a.s.l (as shown in Fig. S1b), the ATL06 product exhibited a more discrete distribution. This likely stems from matching errors that arise when comparing laser points with 30 m resolution SRTM DEM. The findings suggest that the corrected Topo DEM differences exhibit comparable accuracy to ATL06 at these lower elevations. However, at higher elevations (above 5,700 m a.s.l), negative elevation differences were observed in the Topo DEM. These differences are likely related to variations in snow cover, influenced by both seasonal snowfall and potentially atmospheric warming. The significant changes in the off-glacier region at high elevations limit the ability to definitively evaluate the reliability of the Topo DEM using ATL06 data.

It's important to note that despite good agreement with other elevation data sources, uncertainties remain in the Topo DEM at high altitudes (above 5,700 m a.s.l.). This limitation is a common challenge for DEMs derived from historical optical imagery (e.g., Zhou et al., 2018). Factors contributing to this limitation include the low accuracy of the photographic equipment used, a lack of ground control points for precise georeferencing, and seasonal variations caused by random shooting times.

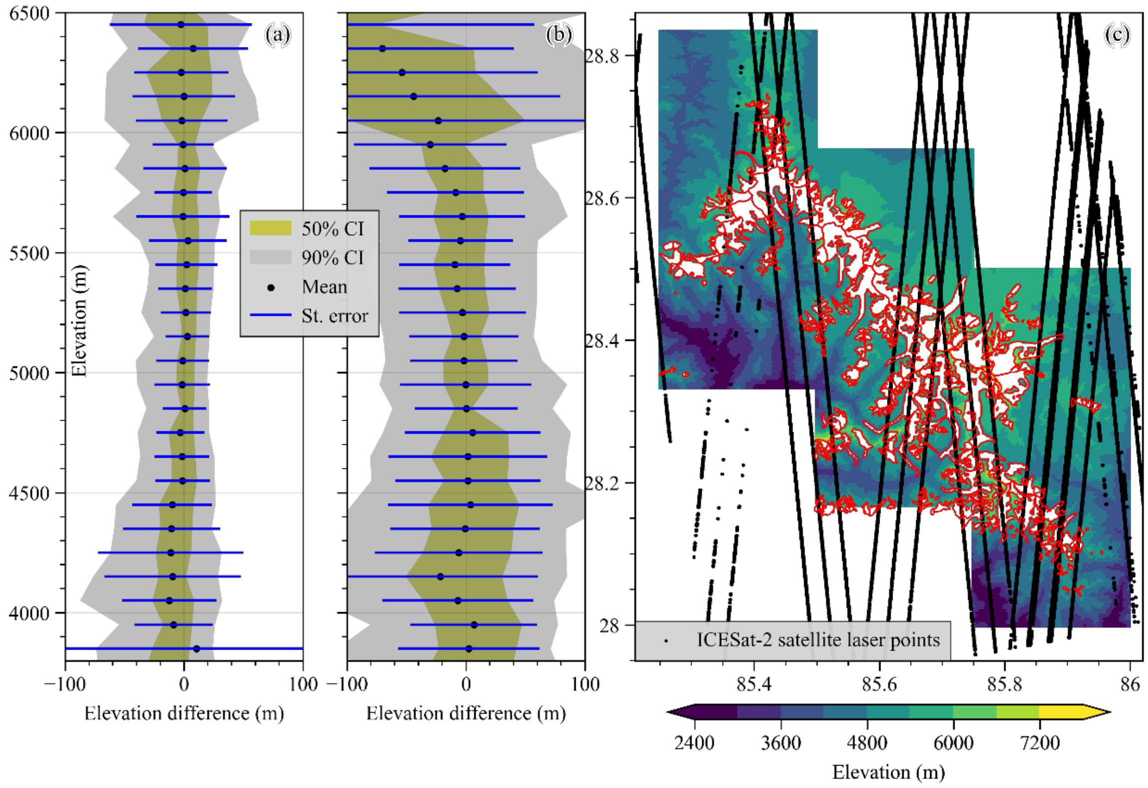

Figure S1. Comparison of Topo DEM (a) and ATL06 (b) elevation differences along altitude (Off-glacier region, Xixiabangma Mountains). Tracks of ATL06 are presented in (c). Elevation zones with fewer than 200 laser spots of ATL06 were excluded from the statistical analysis.

Supplementary Tables

Table S1. The NMAD and Median of elevation difference before (original) and after (co-registration) co-registration processes in off-glacier areas of ETPR

Basin	NMAD		Median	
	original	co-registration	original	co-registration
Ganges	15.22	12.99	-4.96	1.02
Brahmaputra	17.30	14.61	-3.08	0.59
Salween	16.10	12.69	-2.75	0.51
Mekong	17.37	11.97	-6.60	0.53
Yangtze	12.47	8.70	-4.95	0.40
Yellow	9.30	7.71	-1.08	0.38
Irrawaddy	42.68	41.65	2.02	-0.20

Table S2. The standard for generating contours from aerial photos (NPSC, GB/T 12343.1-2008).

Landform	Basic contour distance (m)	
	1 : 50000	1 : 100000
Flat ground (Slope < 2° & elevation difference < 80 m)	10 (5)	20 (10)
Hill area (2° ≤ Slope < 6° & 80 m ≤elevation difference < 300 m)	10	20
Mountainous region (6° ≤ Slope < 25° & 300 m ≤elevation difference < 600 m)	20	40
Alpine region (Slope > 25° & elevation difference > 600 m)	20	40

Table S3. Glacier mass balance from previous studies using 1970s KH-9 Metric Camera imagery in the study area.

Region	Mass balance (m w.e. yr^{-1})	Period	Reference
Himalayas (25° - 37°N, 75° - 93°E)	-0.22 ± 0.13	1975 - 2000	Maurer et al. (2019)
Himalayas (25° - 37°N, 75° - 93°E)	-0.25 ± 0.09	1974 - 2000	King et al. (2019)
Langtang (28.10°-28.39°N, 85.50° - 85.80°E)	-0.24 ± 0.08	1974 - 2006	Ragettli et al. (2016)
Gangotri Glacier, Garhwal (30.802°N, 79.147°E)	-0.20 ± 0.01	1968 - 2006	Bhattacharya et al. (2016)
Eastern Himalayas (27.90°- 28.35°N, 89.80° - 90.90°E)	-0.17 ± 0.05	1974 - 2006	Maurer et al. (2016)
Everest area (27.83°-28.17°N, 86.75° - 87°E)	-0.28 ± 0.12 -0.35 ± 0.12	1962 - 2001 2001 - 2018	King et al. (2020)
Everest area (27.83°-28.17°N, 86.75° - 87°E)	-0.32 ± 0.08	1970 - 2007	Bolch et al. (2011)*

* denotes studies using the Corona KH-4

Table S4. Mass balance statistics from Shean's and Brun's Studies. The units of mass balance (MB) and uncertainties are m w.e. yr^{-1}

Region	This study (1970s-2000)		Shean's (2000-2018)		Brun's (2000-2016)		Average (Shean & Brun's)	
	MB	Error	MB	Error	MB	Error	MB	Error
Ganges	-0.38	0.19	-0.34	0.27	-0.31	0.44	-0.33	0.36
Brahmaputra	-0.30	0.14	-0.42	0.37	-0.43	0.46	-0.42	0.41
Salween	-0.26	0.09	-0.52	0.30	-0.63	0.49	-0.57	0.40
Yellow	-0.19	0.09	-0.46	0.26	—	—	-0.46	0.26
Yangtze	-0.22	0.07	-0.40	0.27	-0.35	0.33	-0.37	0.30
Mekong	-0.29	0.09	-0.45	0.31	-0.49	0.41	-0.47	0.36
Irrawaddy	-0.68	0.56	-0.59	0.44	-0.48	0.57	-0.53	0.50

Supplementary Figures

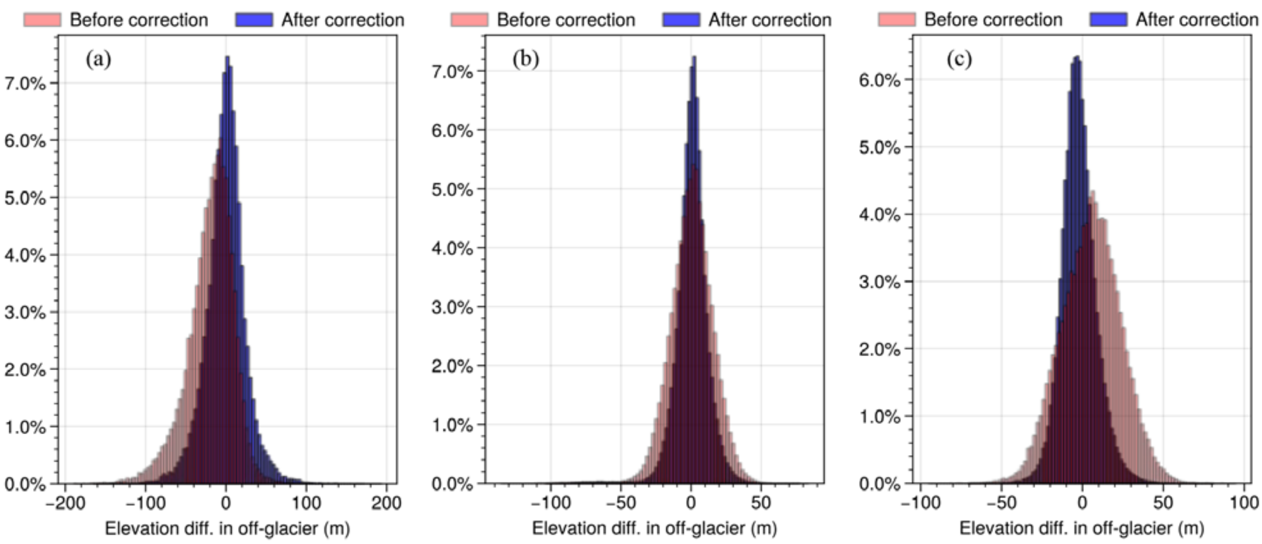

Figure S2. Impact of coregistration and bias correction on off-glacier elevation differences in the ETPR. The vertical axes in all subplots represent the ratio of pixels in each elevation difference zone to the total number of pixels. Briefly, subplots (a), (b), and (c) represent groups with underestimation, low-concentration, and overestimation of elevation difference, respectively.

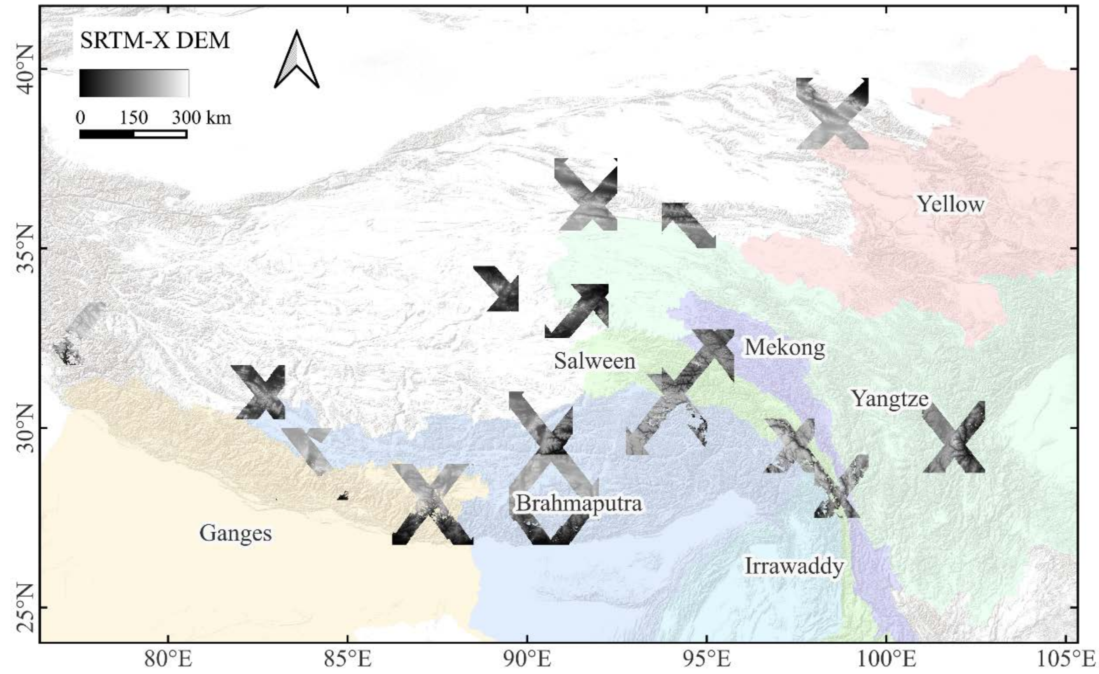

Figure S3. SRTM X-band images used in this study. The base map is sourced from Google Terrain (© Google Maps 2024).

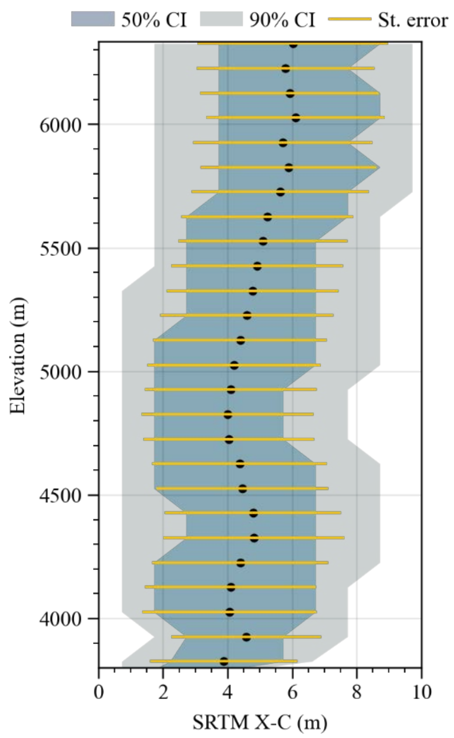

Figure S4. Distribution of the C-X band penetration depth along elevation.

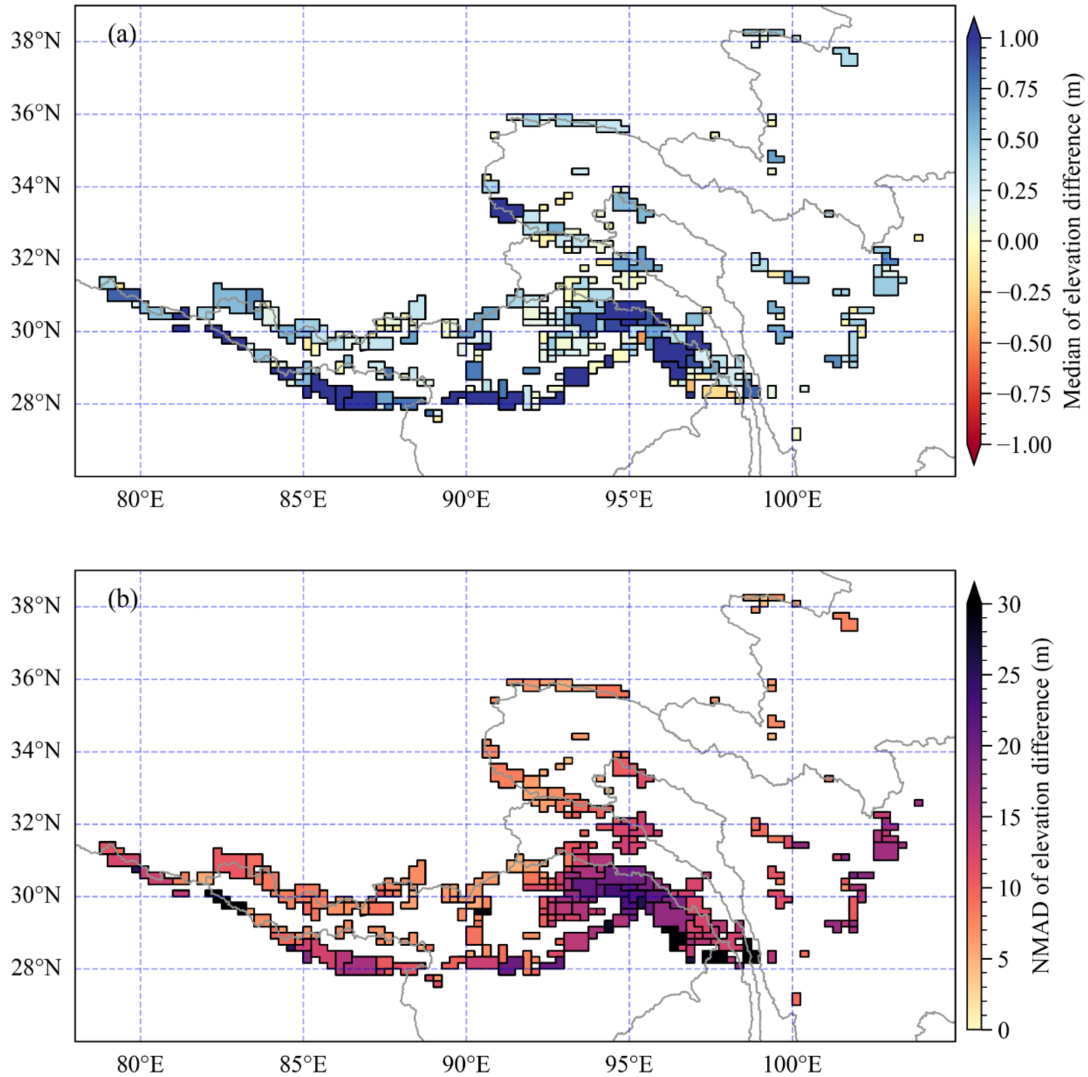

Figure S5. Spatial distribution of median (a) and NMAD (b) of elevation difference in stable areas.

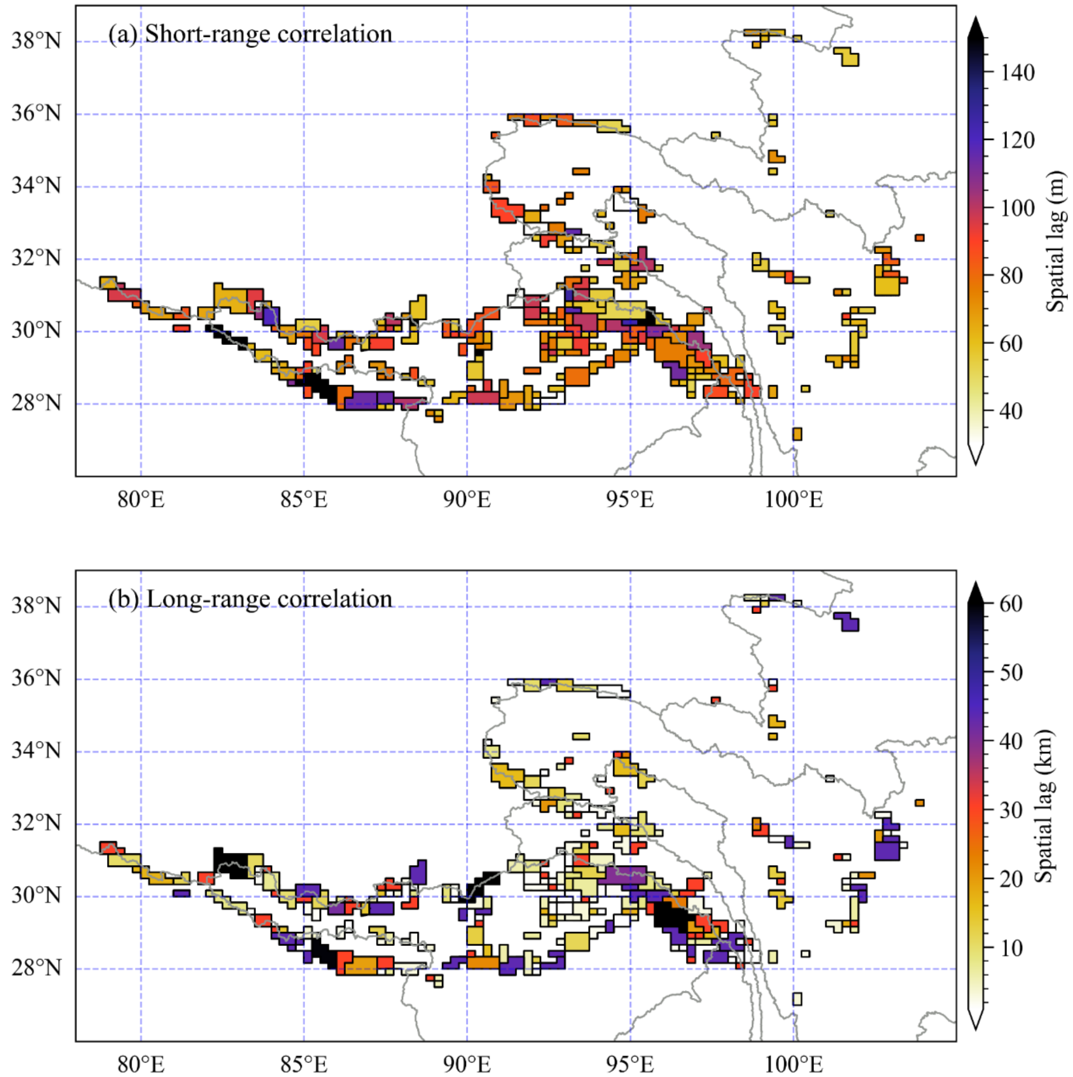

Figure S6. Short-range (a) and long-range (b) correlations of surface elevation difference in different glacier groups. Basin-averaged short-range correlation distance is ~95 m and long-range correlation distance is ~16.26 km.

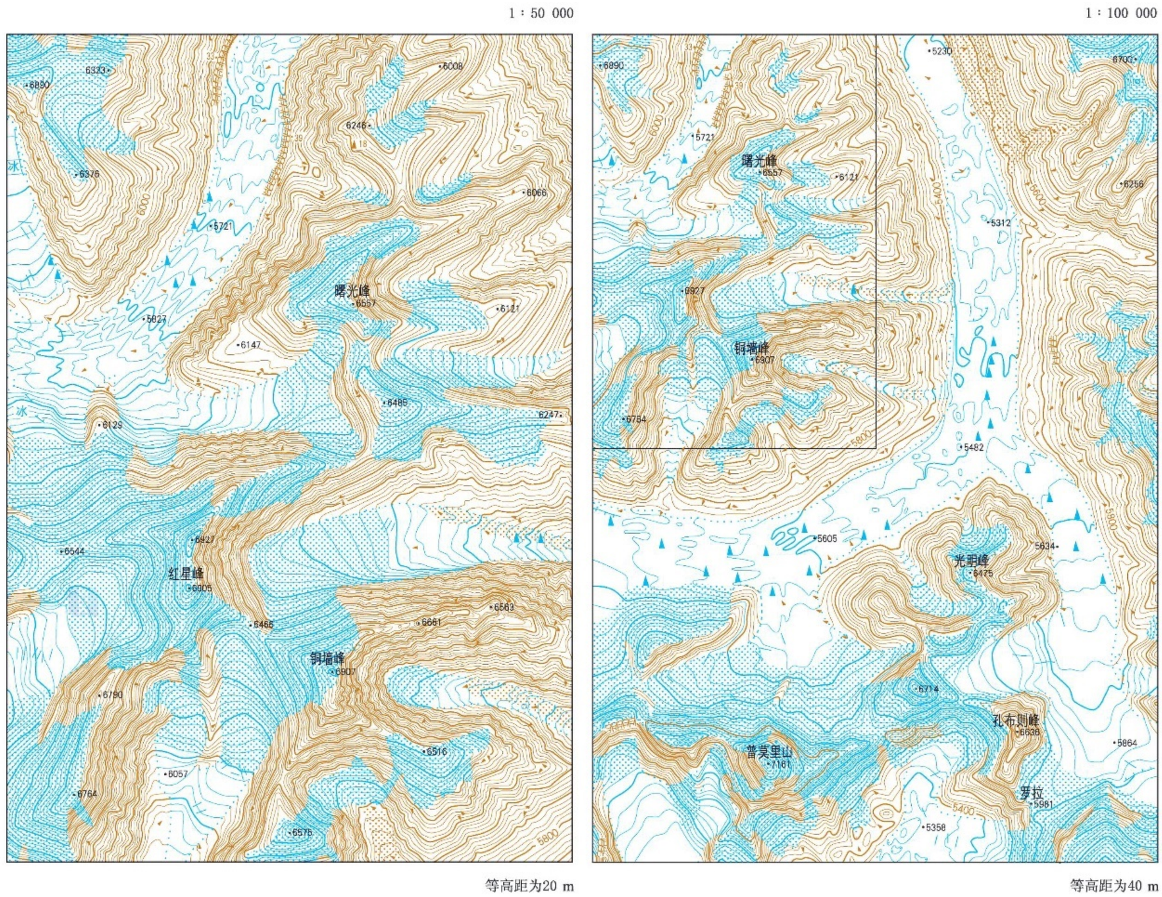

Figure S7. A sample of topographical maps in glacierized region (originate from the NPSC, GB/T 12343.1-2008).

References

Bhattacharya, A., Bolch, T., Mukherjee, K., Pieczonka, T., KropÁČEk, J. A. N., and Buchroithner, M. F.: Overall recession and mass budget of Gangotri Glacier, Garhwal Himalayas, from 1965 to 2015 using remote sensing data, Journal of Glaciology, 62, 1115-1133, https://doi.org/10.1017/jog.2016.96, 2016.

Bolch, T., Pieczonka, T., and Benn, D. I.: Multi-decadal mass loss of glaciers in the Everest area (Nepal Himalaya) derived from stereo imagery, The Cryosphere, 5, 349-358, https://doi.org/10.5194/tc-5-349-2011, 2011.

Brunt, K. M., Neumann, T. A., and Smith, B. E.: Assessment of ICESat-2 Ice Sheet Surface Heights, Based on Comparisons Over the Interior of the Antarctic Ice Sheet, Geophysical Research Letters, 46, 13072-13078, https://doi.org/10.1029/2019gl084886, 2019.

King, O., Bhattacharya, A., Bhambri, R., and Bolch, T.: Glacial lakes exacerbate Himalayan glacier mass loss, Sci Rep, 9, 18145, https://doi.org/10.1038/s41598-019-53733-x, 2019.

King, O., Bhattacharya, A., Ghuffar, S., Tait, A., Guilford, S., Elmore, A. C., and Bolch, T.: Six Decades of Glacier Mass Changes around Mt. Everest Are Revealed by Historical and Contemporary Images, One Earth, 3, 608-620, https://doi.org/10.1016/j.oneear.2020.10.019, 2020.

Maurer, J., Schaefer, J., Rupper, S., and Corley, A.: Acceleration of ice loss across the Himalayas over the past 40 years, Science Advances, 5, eaav7266, https://doi.org/10.1126/sciadv.aav7266, 2019.

Maurer, J. M., Rupper, S. B., and Schaefer, J. M.: Quantifying ice loss in the eastern Himalayas since 1974 using declassified spy satellite imagery, The Cryosphere, 10, 2203-2215, https://doi.org/10.5194/tc-10-2203-2016, 2016.
Ragettli, S., Bolch, T., and Pellicciotti, F.: Heterogeneous glacier thinning patterns over the last 40 years in Langtang
Himal, Nepal, The Cryosphere, 10, 2075-2097, https://doi.org/10.5194/tc-10-2075-2016, 2016.
Smith, B., H. A. Fricker, A. Gardner, M. R. Siegfried, S. Adusumilli, B. M. Csathó, N. H., J. Nilsson, F. S. P., and Team, t. I.-S.: ATLAS/ICESat-2 L3A Land Ice Height (3rd) [dataset], https://doi.org/10.5067/ATLAS/ATL06.003, 2020.
Zhou, Y., Li, Z., Li, J., Zhao, R., and Ding, X.: Glacier mass balance in the Qinghai–Tibet Plateau and its surroundings from the mid-1970s to 2000 based on Hexagon KH-9 and SRTM DEMs, Remote Sensing of Environment, 210, 96-112, https://doi.org/10.1016/j.rse.2018.03.020, 2018.